Applied Physics A (2021) 127:716
https://doi.org/10.1007/s00339-021-04860-8

Applied Physics A
Materials Science & Processing

The effect of a magnetic field on the precipitation of calcium carbonate

Lydia Amer[1] · Salim Ouhenia[1] · Daniel Chateigner[2] · Stéphanie Gascoin[2] · Imad Belabbas[1]

Received: 11 May 2021 / Accepted: 16 August 2021 / Published online: 27 August 2021

Abstract
The effect of a magnetic field on the crystallisation and morphology of $CaCO_3$ in solution was investigated in the 25–80 °C temperature range. The samples were analysed using X-ray diffraction, FTIR, SEM analysis and quantitative analysis based on the Rietveld method. It was demonstrated that the magnetic field, which varied from 50 to 175 mT, had an impact on the polymorphs selectivity and their proportions and on the morphology and the sizes of the $CaCO_3$ particles. It also reduced the overall precipitation rate of $CaCO_3$ minerals in the solution. SEM images showed that the magnetic field modifies the shape of the rhombs of calcite as reflected by the destruction of the particles at 25 and 50 °C with a considerable decrease in their size at 80 °C. These results demonstrate the effectiveness of a magnetic field in reducing the adhesion of calcite to surfaces and thus its possible application in limiting the formation of scale in industrial installations.

Keywords Magnetic fields · Calcium carbonate · Precipitation · Morphology · Quantitative phase analysis · Rietveld method

1 Introduction

Industrial systems are often subjected to scale deposit problems that alter their functioning and lead to serious energetic and economic consequences [1]. Calcium carbonate ($CaCO_3$) is often the main constituent of such scales [2]. Because of its low solubility in water, $CaCO_3$ tends to adhere onto the surfaces. The difficulty of eliminating it using water or other liquid flow is generally associated with the morphology of the three anhydrous polymorphs of $CaCO_3$, i.e. calcite, aragonite and vaterite [3]. The calcite phase produces the most stable and the densest deposits because of its rhombohedral crystal shape. This is contrasted to the needle-like shape of aragonite and the spherical shape of vaterite which make them less adhere to the surfaces and thus easier to eliminate [4]. In order to avoid the scaling phenomenon in industrial devices, chemical treatments with acidic agents are usually used for calcium carbonate removal. The drawbacks of such process are numerous: (i) the high cost, (ii) the negative impact on the environment and on humans, and (iii) the implication in corrosion problems in metal installations [5]. For these reasons, some alternative physical methods have been proposed to tackle the issue of scale deposits [6]. One of these approaches, which consists of using a magnetic field, has emerged as a promising and an efficient one [6]. Hence, investigating the effect of a magnetic field (MF) on the polymorphism of $CaCO_3$ particles has attracted more and more attention.

Lipus and Dobersek [7] observed that applying a MF reduces the thickness of scale on surfaces. Higashitani et al. [8] reported that the MF favours growth rather than nucleation in the precipitation processes. These results were further confirmed by Barrett et al. [9] even if Higashitani et al. [8] poked a major disadvantage of the magnetic treatment in its non-reproducibility. Contrary to Higashitani et al., Holysz et al. [10] reported that the precipitation stage was larger in the absence of MF. Furthermore, it was reported that the effect of a MF and its efficiency depended on diverse parameters like ionic strength, velocity circulation of treated water and magnetic poles geometry. Different pole

✉ Salim Ouhenia
salim.ouhenia@univ-bejaia.dz

✉ Imad Belabbas
imad.belabbas@univ-bejaia.dz

[1] Laboratoire de Physico-Chimie des Matériaux et Catalyse, Université de Bejaia, 06000 Bejaia, Algérie

[2] Laboratoire CRISMAT-ENSICAEN (CNRS UMR 6508), Normandie Université, IUT Caen, Université de Caen Normandie, 6 bd M. Juin, 14050 Caen, France

geometries have been tested by Gabrielli et al. [11] where they reported an increased MF effect efficiency for alternated pole configuration.

Quach et al. [12] have used MF to produce nanobubbles which are known for their cleaning power. They have noticed that MF-generated nanobubbles that bind to $CaCO_3$ nanoparticles would lower the concentration of dissolved $CaCO_3$. On the other hand, it has been reported that the magnetic field influences the physico-chemical properties of the carbonate rocks. An increase in the conductivity of the chalk samples and the variation of the charge of their surfaces have been observed by varying the intensity of the applied field, as well as an increase in the porosity of the rocks caused by the modification of the wettability generated by the magnetised water [13]. Indeed, it is known that MF influences the properties of the exposed solutions such as pH and the conductivity [14]. Experimental results obtained by Liang et al. [15] have shown that the main factor affecting magnetic memory time of $CaCO_3$ solution is the magnetic induction intensity of MF.

Despite the number of research carried out on the subject, the MF action mechanism on $CaCO_3$ precipitation has not been identified yet. Several explanations are proposed in the literature, which are either based on chemical or physical effects. Among those are the modification of the Ca^{2+} and CO_3^{2-}ions hydration [16, 17], the crystallisation process modification due to Lorentz force, and a double layer perturbation in colloidal solutions [8, 18–21]. All these studies agreed that the presence of a MF influenced the crystallisation and nucleation of $CaCO_3$. However, a few quantitative studies about the composition of the polymorphs of $CaCO_3$ were reported. Although the MF might act differently on the various calcium carbonate polymorphs, quantitative analysis of structure, microstructure and volume fraction of each polymorph can be determined routinely.

By studying the effect of MF and different flow rates on precipitation of $CaCO_3$, Sutomo et al. [22] found that for lower flow rate the dominant phase is calcite. When increasing the flow rate, they obtain a mixture of calcite and vaterite with the appearance of a little amount of aragonite at 40 °C. By exposing the solutions of two reactants before mixing them to a magnetic field in quartz cuvette containing magnets, Sronsri et al. [23] obtained a mixture of calcite and aragonite with increasing the proportion of the latter by varying the intensity of the field. However, no presence of vaterite was recorded.

In the present work, we studied the effect of the magnetic field on the precipitation of $CaCO_3$ at three different temperatures (25, 50 and 80 °C), with an applied field up to 0.175 T. All the samples were characterised using X-ray diffraction (XRD) and Fourier-transform infrared spectroscopy (FTIR); both methods are able to discriminate the different polymorphs. Quantitative phase analysis (QPA) was performed using the Rietveld method implemented in the MAUD software [24]. The effect of the MF on the morphology of the crystals was investigated using scanning electron microscopy. The aim of the present study is looking for conditions, in terms of temperature and magnitude of the MF, where: (i) the total quantity of the CaCO3 precipitate is decreased and (ii) the dominant polymorph constituting the precipitate is changed from calcite to vaterite or aragonite, which exhibit morphologies that make them less adhere to surfaces than calcite. These conditions are of great interest and could be adopted in reducing the formation of scale in industrial installations.

2 Materials and methods

Figure 1 represents a schematic diagram of the adopted experimental set-up. Calcium chloride ($CaCl_2$) and potassium carbonate (K_2CO_3) from Prolabo were used as reactants. The chemicals were of analytical grades, i.e. with purity higher than 99%, and were employed without further purification. Precipitation of the crystallised polymorphs was obtained by mixing two 0.1 M/10 ml solutions of $CaCl_2$ and K_2CO_3, prepared using a bidistilled water with a conductivity of 1.6 µS cm^{-1}, at three temperatures of 25, 50 and 80 °C. For each temperature, a magnetic field of 50, 100 and 175 mT was applied using two solenoids between which a beaker containing 10 ml of $CaCl_2$ was inserted and an equivolumetric quantity of K_2CO_3 solution was titrated. The titration was performed after the two solutions were heated up to attain the target temperature. The powder precipitate obtained after filtration was rinsed with double distilled water. Finally, the $CaCO_3$ precipitates were dried at 60° C for 24 h.

The $CaCO_3$ powders were characterised by the X-ray diffraction method (XRD) using Xpert Pro Panalytical diffractometer with the Cu-K1 radiation ($\lambda_{K\alpha1} = 1.5406$ Å) while adopting a scan step of 0.0167°(2θ). The crystallite mean sizes were refined using an isotropic model without microstrain and deconvoluted from the instrument calibration curve. The morphology of the samples was examined using a scanning electron microscope (SEM, JSM-6700 F, JEOL). Fourier transform infrared spectra (FTIR) were acquired on a Shimadzu IRAffinity-1S instrument used in the transmission mode.

2.1 Results

The recorded FTIR spectra of our samples (Fig. 2) were found to be mainly formed by two regions. The spectral region from 500 to 1250 cm^{-1} is characterised by the occurrence of individual sharp peaks which were indexed and used to identify the different polymorphs of $CaCO_3$. The

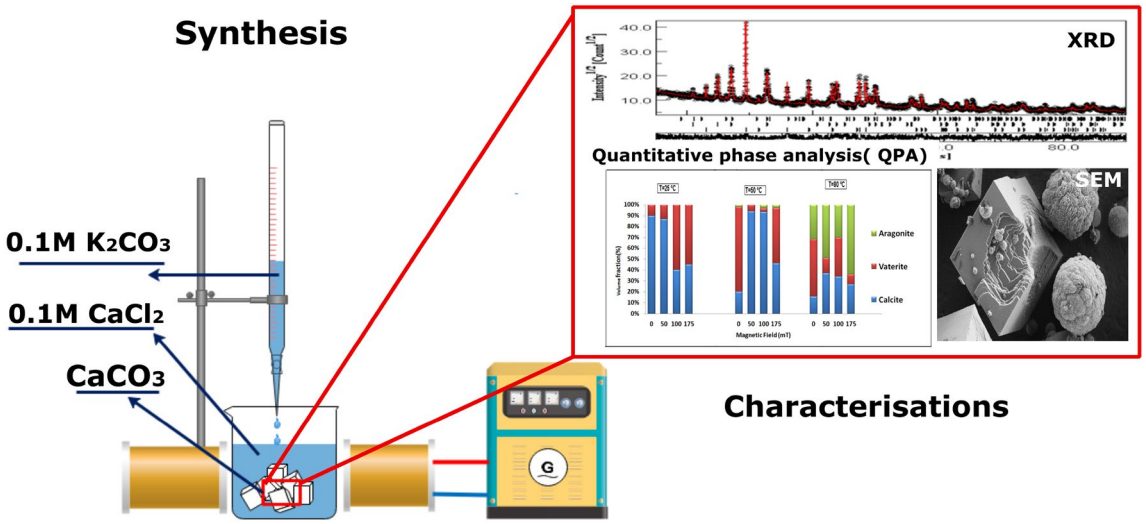

Fig. 1 schematic diagram of the adopted experimental set-up

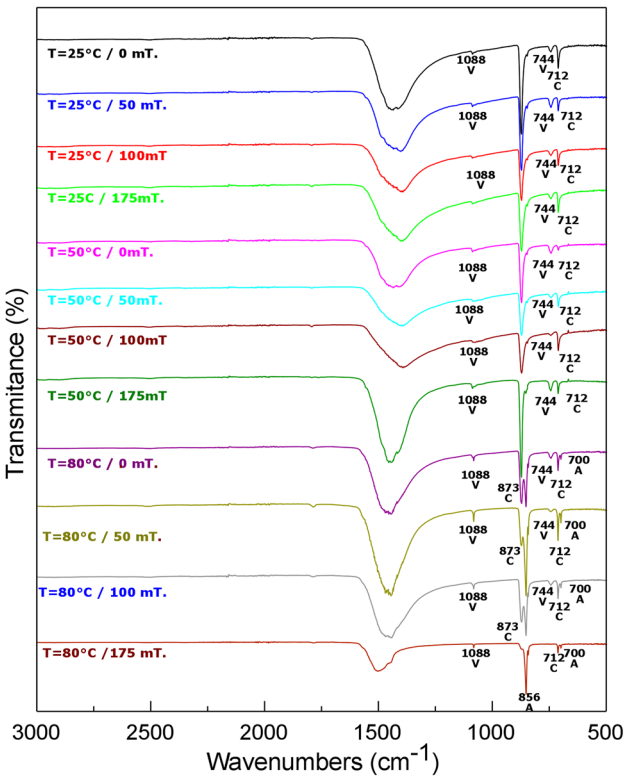

Fig. 2 FTIR spectra of $CaCO_3$ synthesised at different temperatures in the presence or not of a magnetic field

spectral region from 1250 to 1500 cm^{-1} is characterised by the presence of a single broad peak. The latter is formed by the superimposition of several close peaks which are originating from the different polymorphs of CaCO3 (calcite, aragonite, vaterite). Indeed, it is known from the literature that, in the previous spectral region, calcite gives rise to a band at 1435 cm^{-1} [25, 26], vaterite induces four bands at 1424, 1450, 1465 and 1490 cm^{-1} [25, 26], and aragonite gives rise to a band at 1475 cm^{-1} [27]. All these bands were found to be due to an asymmetric C–O stretching mode. The polymorphic composition of our samples varies and depends on the temperature and the magnitude of the applied magnetic field. The amplitude of the broad peak, lying between 1250 and 1500 cm^{-1}, varies as the amplitude of the individual peaks arising from the different polymorphs vary, depending on their volume fractions in the sample. Furthermore, the variation of the amplitudes of the different peaks, related to the different polymorphs, leads to an apparent shift of the maximum of the broad peak. Therefore, the latter peak lying between 1250 and 1500 cm^{-1} was not used to identify the different phases.

2.1.1 Effect of a MF at 25 °C

At $T = 25$ °C, FTIR analysis showed absorption bands at 712 and 873 cm^{-1} attributed to in-plane bending ($\nu 4$) and out-of-plane deformation ($\nu 2$), respectively, corresponding to the absorption bands of calcite. The vaterite phase was also identified with its characteristic bands at 744 and 1088 cm^{-1} [27]. These typical bands were observed in all samples synthesised at 25 °C (Fig. 2). The same phases were revealed by Rietveld quantitative phase analysis (QPA) from XRD diagrams (Fig. 3), confirming that all the samples elaborated at this temperature were composed of a mixture of calcite and vaterite, either in the presence or absence of a magnetic field up to 175 mT. However, the MF changes phase proportions as revealed by the evolution of diffraction peak intensities for these two phases (Fig. 3).

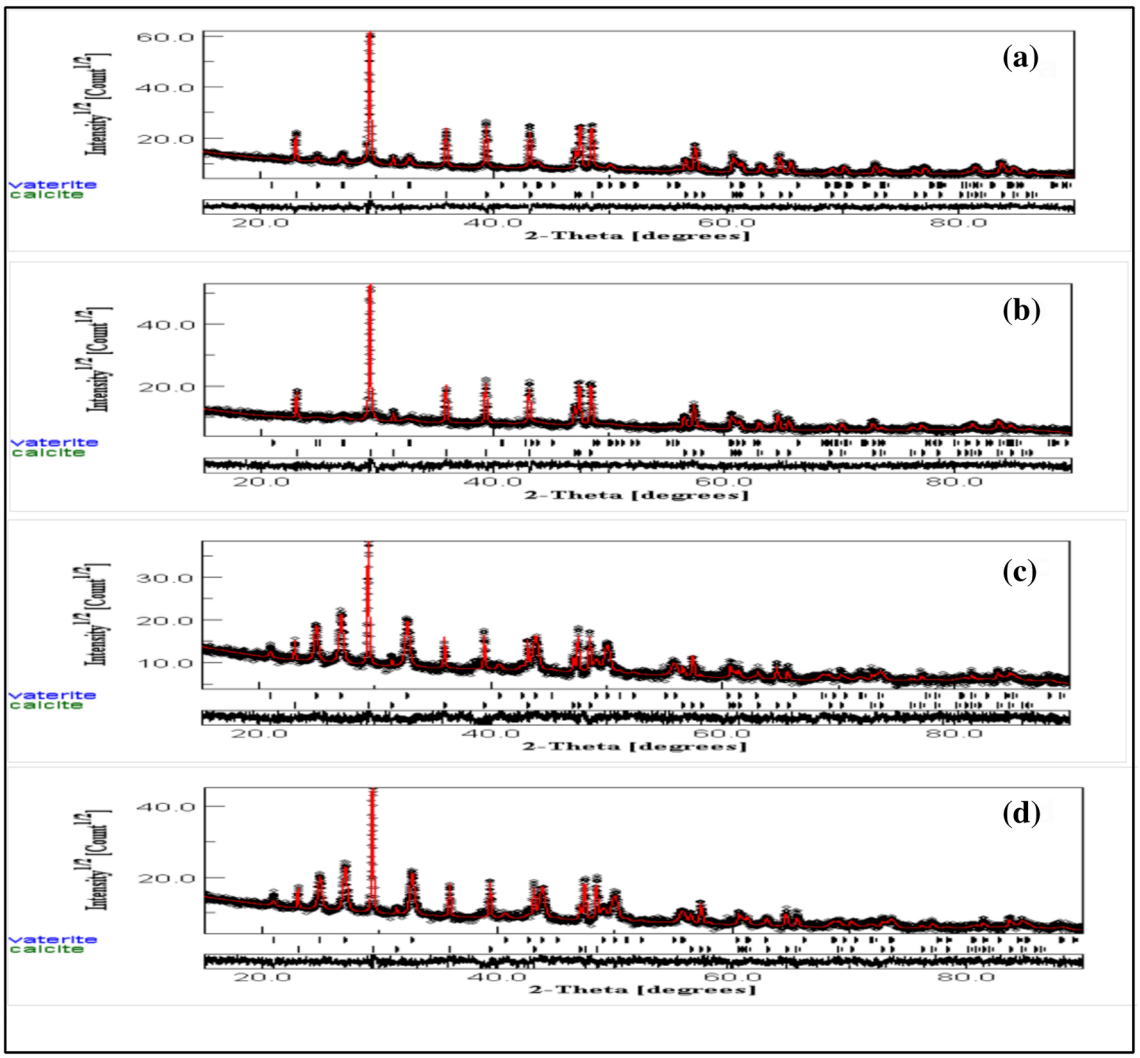

Fig. 3 Calculated (lines), observed (dots), and difference curves after the last cycle of Rietveld refinement for quantitative phase analysis at 25 °C: **a** without MF; **b** at 50 mT; **c** at 100 mT, **d** at 175 mT

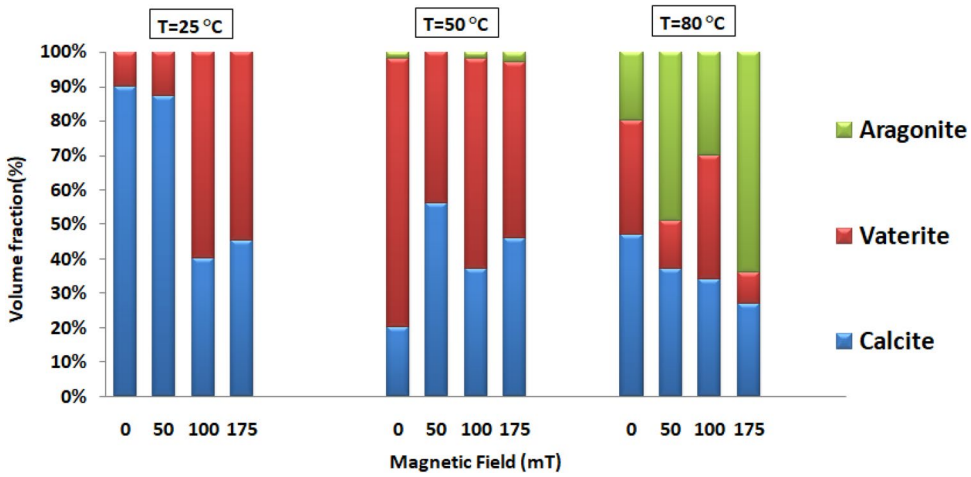

Fig. 4 Volume fraction in the absence and presence of a magnetic field

As shown in Fig. 4, QPA indicated that the volume fraction of calcite varied from 90(1) to 40(2) % and then to 45(2)% when the MF magnitude was changed from 50, 100 to 175 mT, respectively (Table 1). We also observed a significant reduction of the precipitation rate of $CaCO_3$ minerals in the solution with the increase in the magnetic field magnitude. From 100 mT, we considered the vaterite volume fraction as constant, the obtained values being within two standard deviations. The complement to 100% was only associated with vaterite since only these two phases were visible in the diffraction patterns, which varied from 10(1)–60(3) to 55(3)%, respectively. An increase in the crystallites size of the vaterite and calcite phase was also recorded as varying from 335(23) to 519(10) Å for vaterite and from 2315 (59) to 2841(14) Å for calcite (Fig. 5). The SEM images revealed a mixture of calcite rhombs with smooth faces and average particle size of 5.5 µm. In the absence of a MF, SEM images revealed the usual spherical like morphology of vaterite, with an average particle size of 6 µm (Fig. 6a). The formation mechanism of such vaterite morphology arose from two main processes (process I and process II) of the commonly called spherulites growth. In the process I, spherulites grow radially from the nucleation sites with new intermittent branches to fill spaces as much as possible. In process II, the spherulites initially developed as filiform fibres, which then form new branches on the growth front [28]. Andreassen showed that the growth of vaterite spherulites is not achieved by nanoscale aggregation, like sometimes claimed in the literature, but by spherulites types crystal growing [29].

Table 1 Refined parameters obtained by Rietveld refinement and quantitative phase analysis using MAUD

	Phase	a (Å)	b(Å)	C(Å)	Fraction%	Crystallite size(Å)	Rb(%), Rwp (%), Rexp (%)
$T=25$ °C Without MF	Calcite	4.9953(1)		17.084(8)	90(1)	2315 (59)	10.2
	Vaterite	8.469(3)	7.168(4)	4.119(3)	10(1)	335 (23)	11.6 10.4
$T=25$ °C/50 mT	Calcite	4.9909(2)		17.073(1)	87(2)	2601 (62)	10.1, 12.8, 10.2
	Vaterite	8.44 (1)	7.19(2)	4.16 (1)	13(1)	90(8)	
$T=25$ °C /100 mT	Calcite	4.9904 (2)		17.067(1)	40(2)	2740 (10)	10.7, 12.3, 10..9
	Vaterite	8.474(1)	7.150(2)	4.127 (1)	60(3)	481 (10)	
$T=25$ °C/175 mT	Calcite	4.9942 (2)		17.081(1)	45(2)	2841 (12)	10.06, 12.6, 10.3
	Vaterite	8.476(1)	7.155 (2)	4.143 (1)	55(3)	519 (10)	
$T=50$ °C Without MF	Calcite	4.992(2)		17.073(1)	20.(1)	2933 (18)	, 10.7, 11.9 10.2
	Vaterite	8.4724 (9)	7.151(1)	4.125 (1)	78(2)	565 (10)	
	Aragonite	4.97 (1)	7.94(3)	5.72(1)	2(1)	1002(1)	
$T=50$ °C/50 mT	Calcite	4.9944(2)		17.081(1)	56(2)	1555 (44)	10.01,11.2,10.4
	Vaterite	8.473 (1)	7.147(2)	4.131 (1)	44(1)	511(19)	
	Aragonite						
$T=50$ °C/100 mT	Calcite	4.9903 (5)		17.071(2)	37(2)	1557(13)	11.07, 12.4, 11.6
	Vaterite	8.471(1)	7.140 (2)	4.127(1)	61(1)	499(19)	
	Aragonite	4.611 (1)	7.142(1)	5.353(1)	2 (1)	1029(1)	
$T=50$ °C/175mT	Calcite	4.9933(2)		17.034(1)	46 (4)	2254 (77)	10.7, 12.5,10.7
	Vaterite	8.474(1)	7.153(1)	4.126(1)	51(4)	625 (18)	
	Aragonite	4.623 (1)	7.140(1)	5.352(2)	3(1)	1000(10)	
$T=80$ °C Without MF	Calcite	4.9965(3)		17.099 (1)	47(2)	2291 (11)	12.0, 12.6, 10.4
	Vaterite	8.481(1)	7.168 (2)	4.122 (1)	33(2)	586 (29)	
	Aragonite	4.965 (1)	7.990 (3)	5.750 (2)	20(3)	950(30)	
$T=80$ °C/50 mT	Calcite	4.9953 (2)		17.097 (1)	36(2)	2606 (101)	10.7,
	Vaterite	8.483 (2)	7.173(2)	4.117(1)	14(1)	594 (49)	12.8
	Aragonite	4.9646 (5)	7.978(1)	5.753 (7)	49(3)	412(10)	10.2
$T=80$ °C/100 mT	Calcite	4.994(2)		17.082 (1)	34(2)	2463 (111)	10.4, 12.4, 10.3
	Vaterite	8.480(1)	7.165 (1)	4.116 (1)	31(1)	780 (51)	
	Aragonite	4.9625 (7)	7.972 (1)	5.7487 (8)	35(1)	431(12)	
$T=80$ °C/175 mT	Calcite	4.9963 (3)		17.086 (1)	26(2)	2928 (191)	9.6, 12.5, 10.3
	Vaterite	8.487 (3)	7.181(3)	4.119 (2)	9 (1)	964 (186)	
	Aragonite	4.9648(4)	7.9817 (7)	5.7534(4)	64(2)	490(15)	

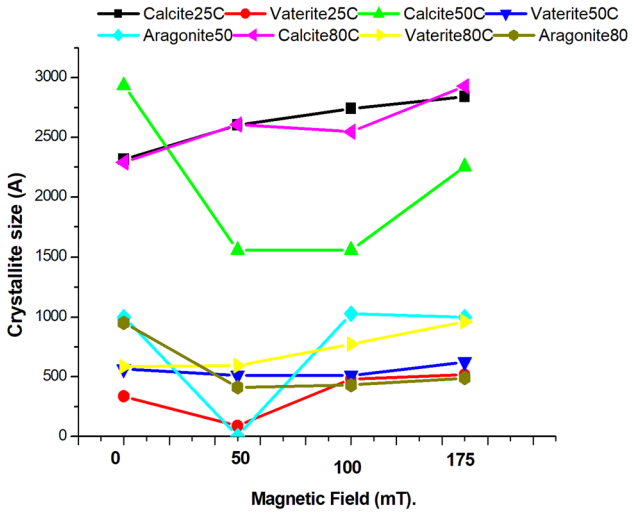

Fig. 5 Mean crystallite sizes of polymorphs in the presence or not of a magnetic field at different temperatures

Under a MF of 100 mT, partial destruction of calcite rhombs occurred, with only average calcite particles around 10 µm remaining. In parallel, nucleation of small spherulitic particles developed with an average size of 1.6 µm on the holes of these rhombs (Fig. 6c, d). The SEM images clearly showed the formation of small crystallites and their agglomeration to form such polycrystalline spherulites. However, the interior of these spherical particles (Fig. 6b) indicated that the formation of the spherulites was initiated by the branching of an elongated prismatic nucleus and not by aggregation of smaller crystallites as reported by Andreasson [29]. Gránàsy et al. [28] assigned this form to the mechanism I, in which radially elongated grains structure is due to a self-organised selection of the grains that have their fast growth direction perpendicular to the interface. However, it has already been reported that the combination of the two mechanisms, i.e. mechanisms I and II, can be simultaneously acting.

The destruction of calcite particles was more accentuated at 175 mT (Fig. 6e). The presence of vaterite spherulites, with an average size of 2.3 µm, was observed. We can also notice a modification in the morphology of part of the vaterite particles from spherulitic to cauliflower-like, accompanied by an increase in their average particles size to 8.3 µm (Fig. 6g). This morphology, typical of the vaterite phase, usually appeared at 50 °C and was due to the agglomeration of small crystallites (Fig. 6f).

Figure 7g shows the formation of intermediate raspberry-like shape particles of vaterite with an average size of 6 µm, which could be formed by the aggregation of several spheres. This morphology was peculiarly interesting since its large porosity could prevent scaling in technical devices.

The smallest calcite crystals were affected in priority by MF applications. Consequently, the mean calcite crystallite sizes reflected the progressive disappearance of the smallest crystals upon field increase. This was indeed what was observed using X-ray diffraction line broadening analysis (Fig. 3), with an increase in calcite crystallite sizes from typically 2200 Å at zero field, up to 2750 Å at 175 mT (Fig. 5). This observation, with the simultaneous increase in vaterite crystallite sizes, clearly identified the growth of the latter at the expense of the former.

At $T = 25$ °C, FTIR analysis showed absorption bands at 712 and 873 cm^{-1} attributed to in-plane bending ($\nu 4$) and out-of-plane deformation ($\nu 2$), respectively, corresponding to the absorption bands of calcite. The vaterite phase was also identified with its characteristic bands at 744 and 1088 cm^{-1} [27]. These typical bands were observed in all samples synthesised at 25 °C (Fig. 2). The same phases were revealed by Rietveld quantitative phase analysis (QPA) from XRD diagrams, confirming that all the samples elaborated at this temperature were composed of a mixture of calcite and vaterite, either in the presence or absence of a magnetic field up to 175 mT. However, the MF changes phase proportions as revealed by the evolution of diffraction peak intensities for these two phases (Fig. 3). As shown in Fig. 4, QPA indicated that the volume fraction of calcite varied from 90(1) to 40(2)% and then to 45(2)% when the MF magnitude was changed from 50, 100 to 175 mT, respectively (Table 1). We also observed a significant reduction of the precipitation rate of $CaCO_3$ minerals in the solution with the increase in the magnetic field magnitude. From 100 mT, we considered the vaterite volume fraction as constant, the obtained values being within two standard deviations. The complement to 100% was only associated with vaterite since only these two phases were visible in the diffraction patterns, which varied from 10(1) to 60(3)%, to 55(3)%, respectively. An increase in the crystallites size of the vaterite and calcite phase was also recorded as varying from 335(23) Å to 519(10) Å for vaterite and from 2315 (59) to 2841(14) Å for calcite (Fig. 5). The SEM images revealed a mixture of calcite rhombs with smooth faces and average particle size of 5.5 µm. In the absence of a MF, SEM images revealed the usual spherical like morphology of vaterite, with an average particle size of 6 µm (Fig. 6a). The formation mechanism of such vaterite morphology arose from two main processes (process I and process II) of the commonly called spherulites growth. In the process I, spherulites grow radially from the nucleation sites with new intermittent branches to fill spaces as much as possible. In process II, the spherulites initially developed as filiform fibres, which then form new branches on the growth front [28]. Andreassen showed that the growth of vaterite spherulites is not achieved by nanoscale aggregation, like sometimes claimed in the literature, but by spherulites types crystal growing [29].

Under a MF of 100 mT, partial destruction of calcite rhombs occurred, with only average calcite particles around 10 µm remaining. In parallel, nucleation of small spherulitic particles developed with an average size of 1.6 µm on the holes of these rhombs (Fig. 6c, d). The SEM images clearly showed the formation of small crystallites and their agglomeration to form such polycrystalline spherulites. However, the interior of these spherical particles (Fig. 6b) indicated that the formation of the spherulites was initiated by the branching of an elongated prismatic nucleus and not by aggregation of smaller crystallites as reported by Andreasson [29]. Gràndsy et al. [28] assigned this form to the mechanism I, in which radially elongated grains structure is due to a self-organised selection of the grains that have their fast growth direction perpendicular to the interface. However, it has already been reported that the combination of the two mechanisms, i.e. mechanisms I and II, can be simultaneously acting.

The destruction of calcite particles was more accentuated at 175 mT (Fig. 6e). The presence of vaterite spherulites, with an average size of 2.3 µm, was observed. We can also notice a modification in the morphology of part of the vaterite particles from spherulitic to cauliflower-like, accompanied by an increase in their average particles size to 8.3 µm (Fig. 6g). This morphology, typical of the vaterite phase, usually appeared at 50 °C and was due to the agglomeration of small crystallites (Fig. 6f).

Figure 6g shows the formation of intermediate raspberry-like shape particles of vaterite with an average size of 6 µm, which could be formed by the aggregation of several spheres. This morphology was peculiarly interesting since its large porosity could prevent scaling in technical devices.

The smallest calcite crystals were affected in priority by MF applications. Consequently, the mean calcite crystallite sizes reflected the progressive disappearance of the smallest crystals upon field increase. This was indeed what was observed (Fig. 5) using X-ray diffraction line broadening analysis, with an increase in calcite crystallite sizes from typically 2200 Å at zero field, up to 2750 Å at 175 mT. This observation, with the simultaneous increase in vaterite crystallite sizes, clearly identified the growth of the latter at the expense of the former.

2.1.2 Effect of a MF at 50 °C

In the absence of MF, QPA (Fig. 8) showed that the powder was composed mainly of vaterite and calcite with a little amount of aragonite. The volume fractions of the three polymorphs were 78(1) %, 20(2) % and 2(1) %, respectively (Fig. 4). The presence of the three phases was confirmed by FTIR analysis (Fig. 2) with the characteristic peaks of aragonite at 700 cm^{-1} and 854 cm^{-1} corresponding to in-plane ($\nu 4$) and out-of-plane ($\nu 2$) bending, respectively, in addition to those of calcite and vaterite. SEM images of the sample synthesised without MF showed small rhombs particles of calcite with smooth faces, cauliflower-shaped particles of vaterite and needle-shaped particles of aragonite (Fig. 9a). The latter morphology was the most common for aragonite which is due to the rapid crystallisation along the [001] direction.

With the application of a 50 mT MF, the powder was composed of 56(2) % of calcite and 44 (1)% of vaterite, without aragonite, i.e. typically less than 0.5% within our resolution (Fig. 4). This was confirmed by FTIR measurements (Fig. 2) and SEM images, with neither aragonite-specific vibrations nor distinct particle shapes for this phase (Fig. 9b). The SEM images revealed the agglomeration of vaterite particles onto calcite ones with an average particles size of 1.8 µm having grown on the calcite rhombs (Fig. 9b). As observed at $T = 25$ °C, this showed that the growth of vaterite was favoured at the expense of calcite. Figure 5c shows vaterite particles with cauliflower morphology and an average particle size of about 12 µm. This form consisted of groups of pellets originating from the centre of a spherical aggregate [30]. A decrease in mean calcite crystallites size from 2900(200) Å to 1550(140)Å was also recorded for this MF (Fig. 5). Increasing the magnitude of the MF to 175 mT results in a powder with 51(4) % of vaterite and 46(5) % of calcite (Table 1), with a small reappearance of the aragonite phase (Fig. 8) with a volume fraction of 3(1) % (Fig. 4). The enhancement of the vaterite crystallites size to 625(18) Å was also observed (Fig. 5). At this temperature, the overall precipitation rate of the CaCO3 minerals also decreased significantly in the systems with the increase in the magnetic field. The effect of the MF on the morphology of particles gave rise to interesting results, with calcite rhombs no longer exhibiting flat and smooth faces are flattened and cored in their centres where vaterite particles grew, up to complete disappearance of calcite (Fig. 9d). This indicated that the presence of a magnetic field considerably altered the growth of calcite at this temperature. This result could be explained by the Lorentz force exerted by the field which may have created a disturbance in the solution and changed the distribution of ions that hindered their access into the nucleation site; which can limit the growth of this polymorph [18, 21]. These results show that the presence of a magnetic field at this temperature affects mainly the shape regularity and integrity of the rhombs of the calcite phase. Thus, one could easily imagine that the appearance of holes and large porosities on their surfaces and bulks could hinder their adhesion on surfaces.

2.1.3 Effect of a MF at 80 °C

At this temperature, the samples were all composed of a mixture of the three polymorphs whatever the applied MF.

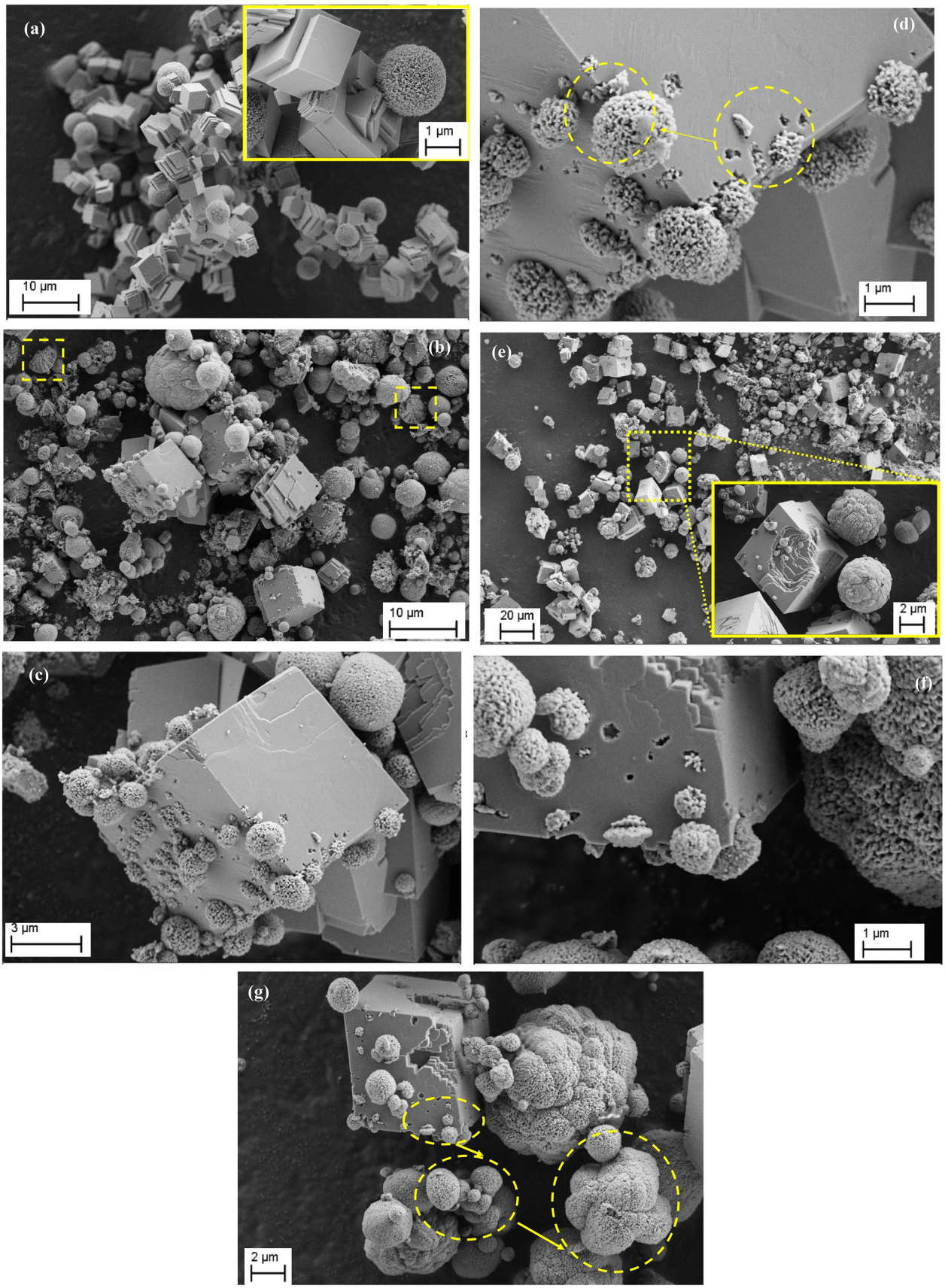
(a)
1 µm
10 µm
(d)
1 µm
(b)
10 µm
(e)
20 µm
2 µm
(c)
3 µm
(f)
1 µm
(g)
2 µm

◂**Fig. 6** SEM images of $CaCO_3$ particles synthesised at 25 °C. **a** calcite rhombs and spheric vaterite in the absence of MF **b** calcite and vaterite at 100 mT (**c**, **d**). **e** Destruction of rhombs of calcite and cauliflowers shape of vaterite at 175 mT. **f** Nucleation of small crystallites of vaterite on calcite particles at 100 mT **g** formation of intermediate raspberry-like shapes at 175 mT

QPA (Fig. 7) and FTIR analyses (Fig. 2) attested that, in the presence of MF, a considerable increase in aragonite phase fraction occurs, almost tripled from 20(3) % to 64(2) % at 175 mT, with a decrease in its crystallites size from 950(30) Å to 490(15) Å (Fig. 5).

In the absence of a MF, SEM images (Fig. 10) revealed a mixture of regular calcite rhombs, with relatively smooth faces and an average particle size of 7.6 µm, and usual acicular aragonite particles. We also noticed the presence of super-structured rosettes of vaterite. Such morphology is developed generally from small needle-like particles (Fig. 10a). Qi et al. [31] reported that the formation of this structure occurs via colloidal intermediate and mesoscale transformation with crystalline structures which are constructed and/or transformed from larger units instead of single ions. Crystals are assembled then from nanobuilding units in three-dimensional orientations to form so-called mesocrystals [31]. Under 50 mT, no change in the morphology of the aragonite and calcite was observed, with, however, a decrease in calcite means particles size to 0.8 µm (Fig. 10b, c).

Under 100 mT, SEM images (Fig. 10e) showed such aggregations clearly forming super-structured rosettes or snowflake shape particles (Fig. 10d). At this temperature, very thin petal-like vaterite particles were obtained (Fig. 10d). The thickness of the petals (Fig. 10e) is the consequence of a fast growth as it was reported by Sand et al. [32]. We can also distinguish nearly intact calcite particles with an average size of 2.7 µm. As under 50 mT, we observed the appearance of small rectangular particles with an average size of 0.7 µm.

At 80 °C, we noticed that the MF field favours the formation of both aragonite and vaterite at the expense of calcite. These results along with the alteration of calcite rhombs at 25 and 50 °C can be translated as the efficiency of the magnetic field to eliminate or at least severely transform calcite while promoting vaterite formation with various morphologies. It is clear that smaller and more porous calcite particles are easier to move than densest ones obtained without MF applications. It should be remembered that the two aragonite and vaterite phases adhere less than calcite and are, therefore, easier to remove by water circulation flow. According to Alabi et al. [33], the efficiency of the magnetic field lies precisely in the formation of these unstable phases that are more soluble and easier to eliminate. At this temperature, we also observe that the precipitation rate of $CaCO_3$ decreases drastically with the increase in the magnetic field.

3 Discussion

Our results showed that the presence of a MF reduces the overall precipitation rate of $CaCO_3$ and alters calcite growth. The latter effect is clearly evidenced in SEM images by revealing perturbed calcite rhombs at 25 and 50 °C as soon as a MF was applied during the precipitation. Also, at 80 °C, the average calcite particle size decreased from 7.5 µm at zero field to 0.8 µm and 0.7 µm under 50 and 100 mT, respectively. We should remind that calcite is the major component of the limestone. The mechanism by which the MF influences the formation and growth of a given phase remains difficult to elucidate. Nevertheless, the Lorentz force hypothesis causing double ionic layers distortion of the colloids, thus influencing nucleation, is the most plausible to explain the results presented here. Indeed, during the synthesis, in the presence of a MF, it was observed that the precipitate remains suspended on the surface of the water and does not fall to the bottom of the beaker. This was the result of the Lorentz force exerted by the MF.

Coey et al. reported that the MF has no direct effect on water chemistry, as claimed by other authors [17], but rather alters the morphology of the $CaCO_3$ particles and their adhesion to surfaces [34]. Ojaniemi et al. [35] have studied by simulations the adhesion of the calcite particles to the walls of equipment. They reported that the adhesion is controlled by colloidal interaction forces, like DLVO (Derjaguin-Landau-Verwey-Overbeek) forces, which appear between charged surfaces interacting through a liquid medium [35]. The adhesion is driven by the balance between repulsive and attractive forces involved by the particles of the electrical layers surrounding the colloid. Indeed, when a particle is immersed in an electrolytic solution, an electrical double layer, called stern and diffusion layers, is formed around it. So for aggregation to occur, the particles must overcome the energy barrier created by the two layers, which is sensitive to both ion strength and the size of the particles. At high ionic strength, the crushing of the diffusion layer occurs. This reduces the repulsive forces and therefore favours the aggregation. For small particle size, fouling occurs even for the lowest ionic strength. However, the energy barrier created by the two layers could be overcome thanks to thermal agitation and the Brownian movement.

In the presence of a magnetic field, all ionic species are under the effect of the Lorentz force which modifies their distribution in the two layers as well as their mutual interactions. The resulting stress influences the exchange between the $CaCO_3$ particles and the Ca^{2+} and CO_3^{2-}free-ions present in the solution. This gives rise to a modification of the

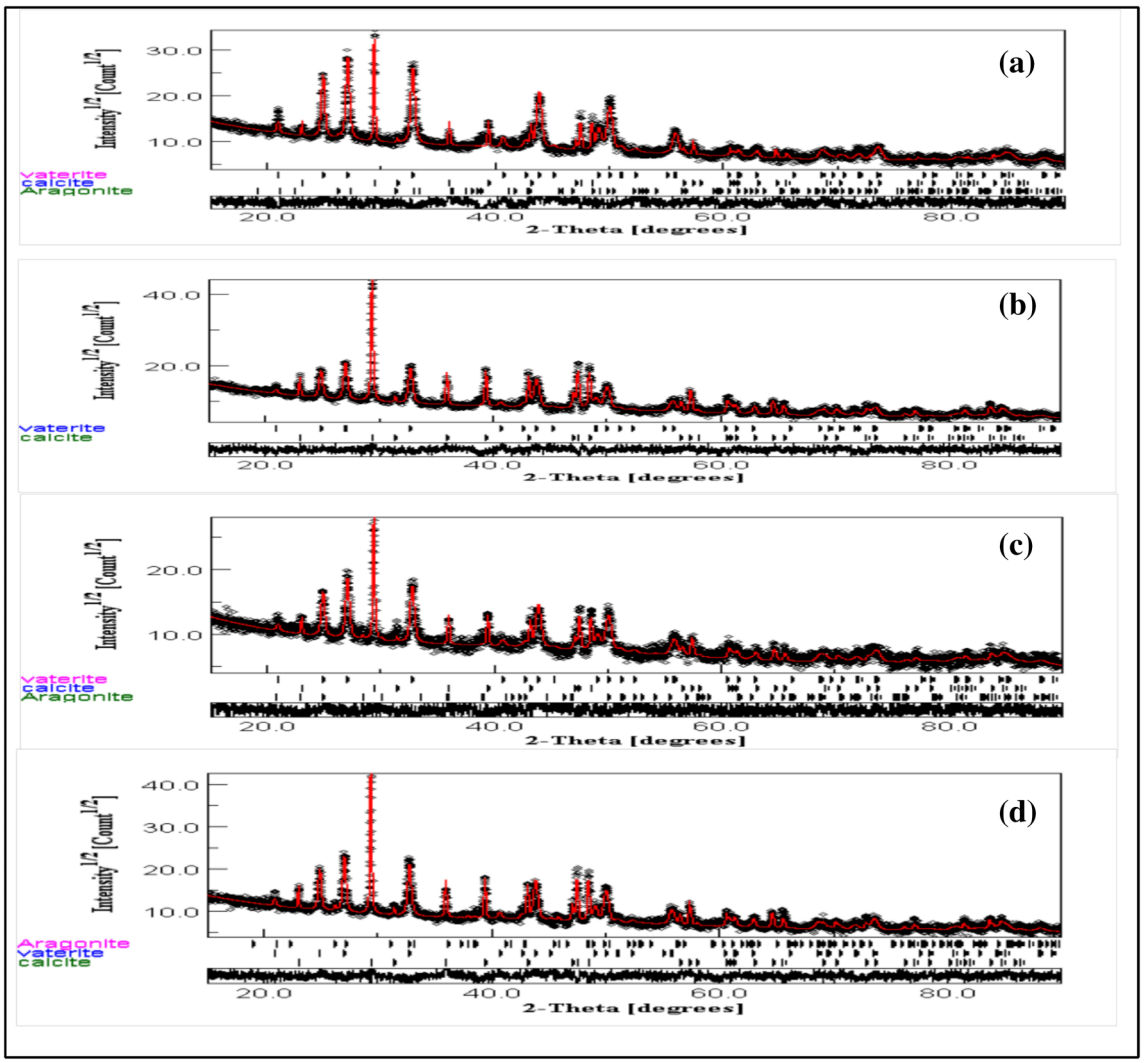

Fig. 7 Calculated (lines), observed (dots), and difference curves after the last cycle of Rietveld refinement for quantitative phase analysis at 50 °C: **a** without MF; **b** at 50 mT; **c** at 100 mT, **d** at 175 mT

composition of the $CaCO_3$ particles' surfaces. The surface composition plays a major role in both dissolution and precipitation of $CaCO_3$ particles [36] and influences directly the resulting precipitated $CaCO_3$ polymorph, since the atomic configuration of the three polymorphs ending surfaces is different. This may explain the observed modifications in the growth and the precipitation of $CaCO_3$particles in the presence of a MF, in terms of polymorph type, polymorphs proportions and their morphologies.

We have clearly demonstrated that the application of a MF has an impact in defining the nature of polymorphs as well as their proportions in the precipitated $CaCO_3$. Indeed, at 25 °C, the application of a MF, of magnitude larger than 100 mT, allows enhancing by about a factor of 5 the proportion of vaterite, compared to precipitation in zero field. Otherwise, at 80 °C, the application of a MF leads to an increase in the quantity of aragonite in the precipitated $CaCO_3$. The proportion of the latter polymorph was increased by a factor 3 by applying a MF with a magnitude of 175 mT, compared to the reference sample.

Globally, our results showed that the application of a MF, at 25 and 80 °C, leads to a decrease in the calcite fraction and the overall precipitation rate of $CaCO_3$ minerals in the solution. The most important decrease in calcite fraction, by a factor 5, was recorded at 25 °C with a magnitude of the MF larger than 100 mT.

It has been observed that the magnetic field influences the morphology of vaterite. By varying the magnitude of the MF and the temperature, the morphology varies from spheroids to rosettes, cauliflower and petal as can be seen from SEM images. It is known that, for a given morphology, particle growth is enhanced when enough material is supplied from the solution that continuously reaches the growing faces of aggregates, while all the nuclei that are

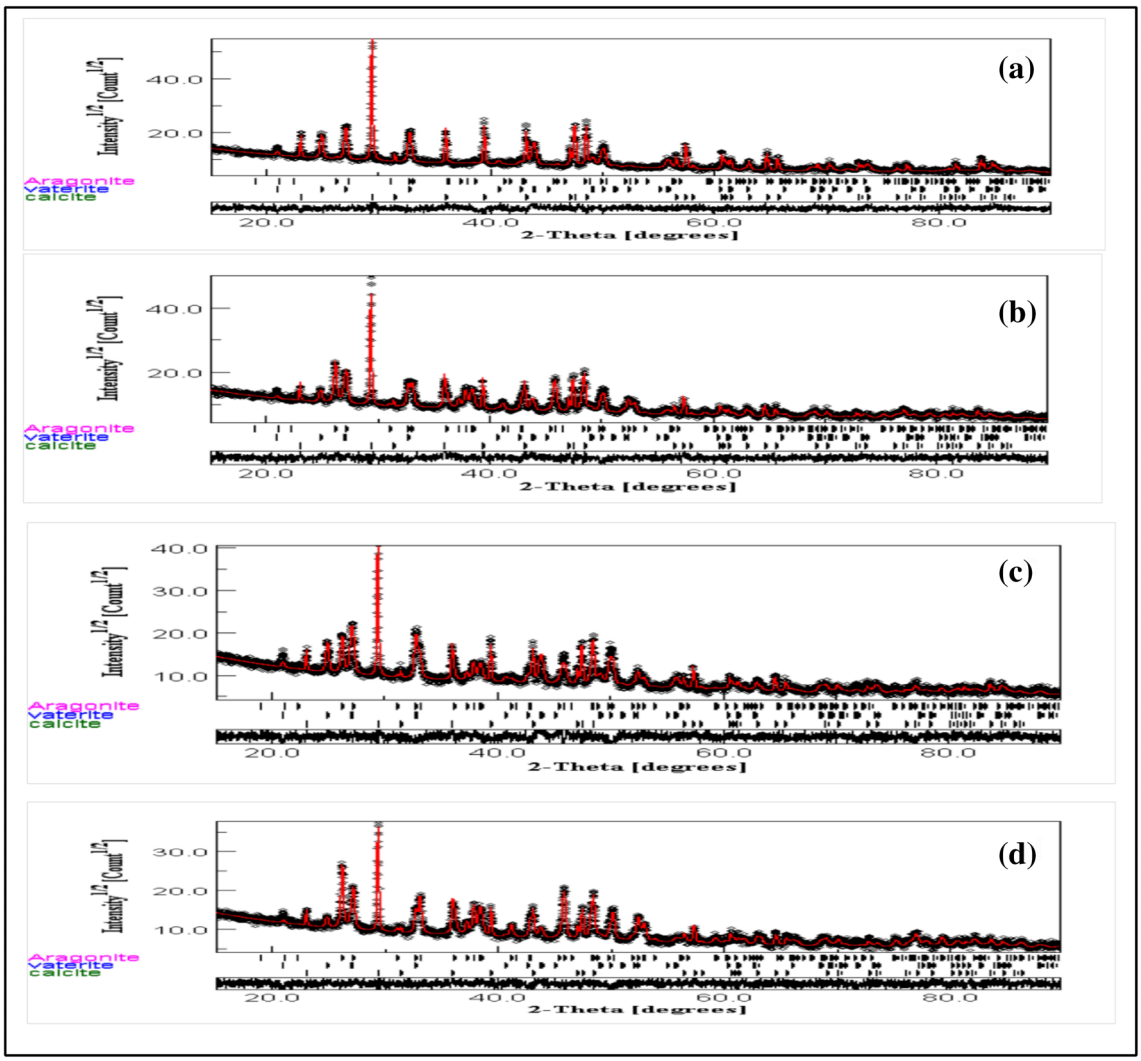

Fig. 8 Calculated (lines), observed (dots), and difference curves after the last cycle of Rietveld refinement for quantitative phase analysis at 80 °C: **a** without MF; **b** at 50 mT; **c** at 100 mT, **d** at 175 mT

not aligned with the fastest-growing direction are eliminated. Although it is not obvious to accurately explain how a magnetic field influences the morphology of vaterite particles, one could correlate its effect to that of the Lorentz force that influences the exchange between the $CaCO_3$ particles and the Ca^{2+} and CO_3^{2-} free ions present in solution.

The fact that the magnetic field can have a different effect at different temperatures can be explained by the following. The magnetic field impacts the formation of the $CaCO_3$ polymorphs by acting on the Ca^{2+} and CO_3^{-2} free ions present in the solution via the Lorentz force. The latter has a magnitude which depends on both the velocity of ions and the magnitude of the applied magnetic field. When varying the temperature the thermal agitation within the solution changes which obviously impacts the motion (velocities and trajectories) of the Ca^{2+} and CO_3^{-2} free ions. Then, this will modify the action of the magnetic field, through the Lorentz force, on the formation of the $CaCO_3$ polymorphs.

4 Conclusion

In this study, the effect of a magnetic field, for which the magnitude varied from 0 to 175 mT, on the crystallisation and morphology of $CaCO_3$ was investigated using a quantitative phase analysis based on the Rietveld method. The results showed that the presence of a MF alters the growth of the calcite phase. This was clearly observed through the decrease in its volume fraction at ambient temperature and in the destruction of the rhombs of its particles at 25 and 50 °C as it has been revealed by SEM images. The presence of a MF also reduces the overall precipitation rate of $CaCO_3$ and influences the formation of the vaterite phase. In addition to

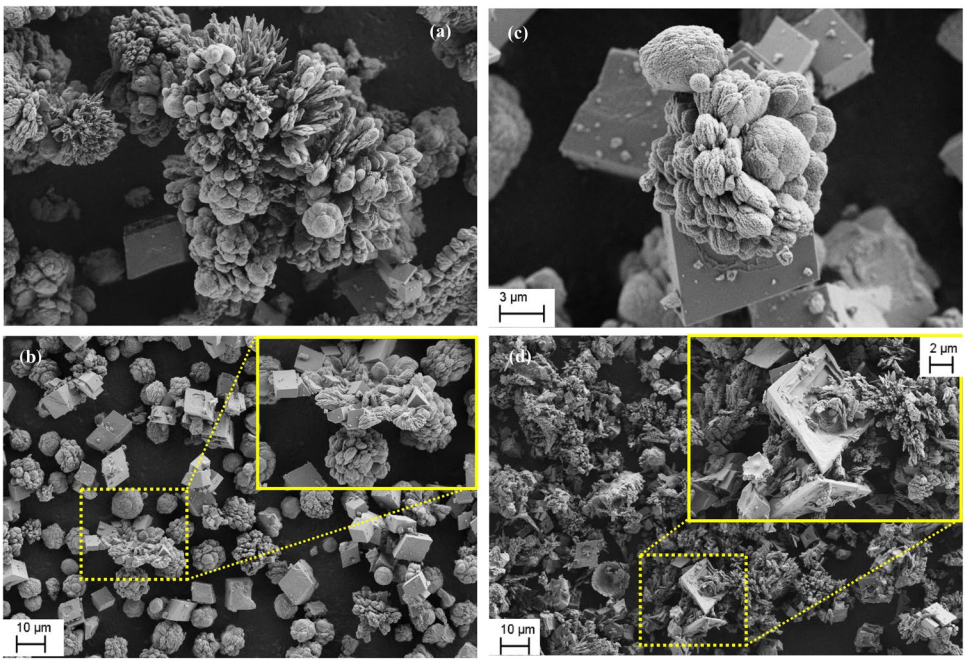

Fig. 9 SEM images of $CaCO_3$ particles synthesised at 50 °C. **a** Calcite rhombs and cauliflowers of vaterite and needle shape of aragonite in absence of MF. **b** Regular rhombs of calcite and vaterite at 50 mT **c** Cauliflowers of vaterite at 50 mT. **d** The flattening and venting of the rhombs of calcite at 175 mT

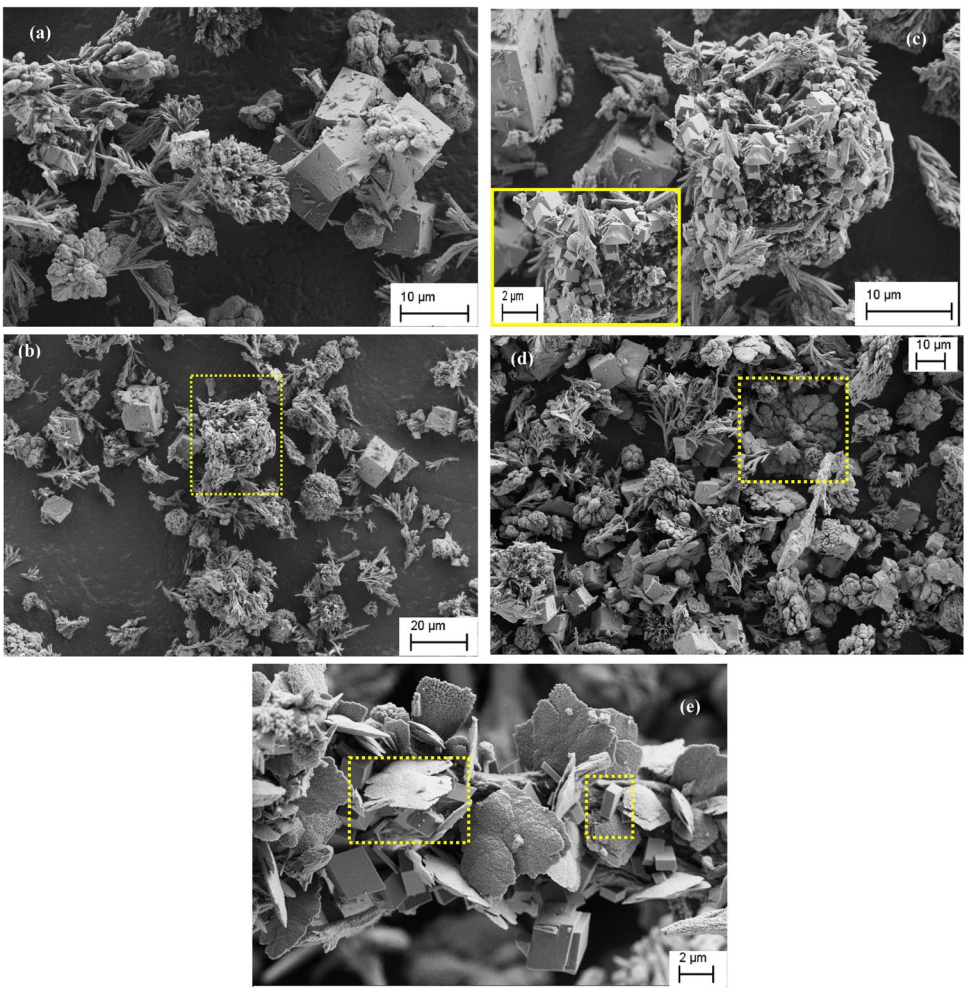

Fig. 10 SEM images of $CaCO_3$ particles synthesised at 80 °C. **a** calcite rhomb and cauliflowers of vaterite and needle shape of aragonite in absence of MF. **b** SEM images of $CaCO_3$ particles synthesised at 50 mT. **c** A small regular cubes of calcite at 50 mT. **d** SEM images of $CaCO_3$ particles synthesised at 100 mT. **e** Petal forms of vaterite and cubic and small rectangular of calcite particles at 100 mT

the increase in its volume fraction at ambient temperature, vaterite particles can be piled up into diverse morphologies ranging from spherical, super-structured rosettes to very fine petal form, by varying the intensity of the magnetic field.

Acknowledgements Authors acknowledge the University of Bejaia and la Direction Générale de la Recherche Scientifique et du Développement Technologique (DGRSDT) for funding. This work was achieved in the framework of the PRFU project No. B00L02UN060120180005.

Declaration

Conflict of interest The authors declare that they have no known competing for financial interests or personal relationships that could have appeared to influence the work reported in this paper.

References

1. A. Fathi et al., Effect of a magnetic water treatment on homogeneous and heterogeneous precipitation of calcium carbonate. Water Res. **40**(10), 1941–1950 (2006)
2. E. Chibowski, A. Szczes, L. Holysz, Influence of sodium dodecyl sulfate and static magnetic field on the properties of freshly precipitated calcium carbonate. Langmuir **21**(18), 8114–8122 (2005)
3. S. Kobe et al., The influence of the magnetic field on the crystallisation form of calcium carbonate and the testing of a magnetic water-treatment device. J. Magn. Magn. Mater. **236**(1–2), 71–76 (2001)
4. M. Gryta, The influence of magnetic water treatment on CaCO3 scale formation in membrane distillation process. Sep. Purif. Technol. **80**(2), 293–299 (2011)
5. C.Y. Tai et al., Magnetic effects on crystal growth rate of calcite in a constant-composition environment. J. Cryst. Growth **310**(15), 3690–3697 (2008)
6. A. Szkatula, M. Balanda, M. Kopeć, Magnetic treatment of industrial water. Silica activation. Eur. Phys. J.-Appl. Phys. **18**(1), 41–49 (2002)
7. L. Lipus, D.J.C.E.S. Dobersek, Influence of magnetic field on the aragonite precipitation. Chem. Eng. Sci. **62**(7), 2089–2095 (2007)
8. K. Higashitani et al., Effects of a magnetic field on the formation of CaCO3 particles. J. Colloid Interface Sci. **156**(1), 90–95 (1993)
9. R.A. Barrett, S.A. Parsons, The influence of magnetic fields on calcium carbonate precipitation. Water Res. **32**(3), 609–612 (1998)
10. L. Hołysz, M. Chibowski, E. Chibowski, Time-dependent changes of zeta potential and other parameters of in situ calcium carbonate due to magnetic field treatment. Colloids Surf., A **208**(1–3), 231–240 (2002)
11. C. Gabrielli et al., Magnetic water treatment for scale prevention. Water Res. **35**(13), 3249–3259 (2001)
12. N.V.-Y. Quach, A. Li, J.C. Earthman, Interaction of calcium carbonate with nanobubbles produced in an alternating magnetic field. ACS Appl. Mater. Interfaces. **12**(39), 43714–43719 (2020)
13. F. Amrouche et al., Effect of magnetic field on physiochemical properties of carbonate reservoirs. in *82nd EAGE Annual Conference & Exhibition*. European Association of Geoscientists & Engineers. **2020**(1), 1–5 (2020)
14. R. Mghaiouini et al., The electromagnetic memory of water at kinetic condition. Int. J. Curr. Eng. Technol. **10**(1), 11 (2020)
15. Z. Lv et al., Analysis of factors affecting magnetic memory tme of CaCO3 solutions based on orthogonal experiment. Sensors Materials **32**(4), 1339–1350 (2020)
16. S. Knez, C. Pohar, The magnetic field influence on the polymorph composition of CaCO3 precipitated from carbonized aqueous solutions. J. Colloid Interface Sci. **281**(2), 377–388 (2005)
17. A. Szcześ et al., Effects of static magnetic field on water at kinetic condition. Chem. Eng. Process. **50**(1), 124–127 (2011)
18. E. Chibowski, L. Hołysz, A. Szcześ, Adhesion of in situ precipitated calcium carbonate in the presence and absence of magnetic field in quiescent conditions on different solid surfaces. Water Res. **37**(19), 4685–4692 (2003)
19. R. Gehr et al., Reduction of soluble mineral concentrations in CaSO4 saturated water using a magnetic field. Water Res. **29**(3), 933–940 (1995)
20. H.L. Madsen, Influence of magnetic field on the precipitation of some inorganic salts. J. Cryst. Growth **152**(1–2), 94–100 (1995)
21. J. Coey, S. Cass, Magnetic water treatment. J. Magn. Magn. Mater. **209**(1–3), 71–74 (2000)
22. S. Sutomo et al., The morphology aspect of CaCO3 scale impact of solenoid magnetic field in the various flow rate solution in the piping system. Materials Today: Proceedings **13**, 287–292 (2019)
23. C. Sronsri, U. Kongpop, W. Sittipol, Quantitative analysis of calcium carbonate formation in magnetized water. Mater. Chem. Phys. **245**, 122735–122744 (2020)
24. L. Lutterotti, S. Matthies, H. Wenk, MAUD: a friendly Java program for material analysis using diffraction. IUCr: Newsletter of the CPD. **21**, 14–15 (1999)
25. Z.G. Wu et al., Preparation of vaterite CaCO3 microspheres by fast precipitation method. Int. J. Mater. Res. **108**(3), 245–248 (2017)
26. R. Ševčík et al., Characterization of vaterite synthesized at various temperatures and stirring velocities without use of additives. Powder Technol. **284**, 265–271 (2015)
27. S. Gopi, V. Subramanian, K. Palanisamy, Aragonite–calcite–vaterite: A temperature influenced sequential polymorphic transformation of CaCO3 in the presence of DTPA. Mater. Res. Bull. **48**(5), 1906–1912 (2013)
28. L. Gránásy et al., Phase field theory of crystal nucleation and polycrystalline growth: A review. J. Mater. Res. **21**(2), 309–319 (2006)
29. J.-P. Andreassen, Formation mechanism and morphology in precipitation of vaterite—nano-aggregation or crystal growth? J. Cryst. Growth **274**(1–2), 256–264 (2005)
30. K.K. Sand et al., Crystallization of CaCO3 in water–alcohol mixtures: spherulitic growth, polymorph stabilization, and morphology change. Cryst. Growth Des. **12**(2), 842–853 (2011)
31. J.Q. Qi et al., Electric field-controlled crystallizing CaCO3 nanostructures from solution. Nanoscale Res. Lett. **11**(1), 120 (2016)
32. K.K. Sand et al., Crystallization of CaCO3 in water–alcohol mixtures: spherulitic growth, polymorph stabilization, and morphology change. Cryst. Growth Des. **12**(2), 842–853 (2012)
33. A. Alabi et al., Advances in anti-scale magnetic water treatment. Environ. Sci.: Water Res. Technol. **1**(4), 408–425 (2015)
34. J. Coey, S. Cass, Magnetic water treatment. J. Magn. Magn. Mater. **209**(1–3), 71–74 (2000)
35. U. Ojaniemi et al., Wall function model for particulate fouling applying XDLVO theory. Chem. Eng. Sci. **84**, 57–69 (2012)
36. P. Moulin, H. Roques, Zeta potential measurement of calcium carbonate. J. Colloid Interface Sci. **261**(1), 115–126 (2003)